Friction **5**(4): 447–454 (2017)
DOI 10.1007/s40544-017-0158-6
ISSN 2223-7690
CN 10-1237/TH
RESEARCH ARTICLE

Effects of impact energy on the wear resistance and work hardening mechanism of medium manganese austenitic steel

Hui CHEN[1,2], **Dong ZHAO**[1], **Qingliang WANG**[1,*], **Yinghuai QIANG**[1], **Jianwei QI**[1]

[1] *School of Materials Science and Engineering, China University of Mining & Technology, Xuzhou 221116, China*

[2] *Jiangsu Key Laboratory of Large Engineering Equipment Detection and Control, Xuzhou Institute of Technology, Xuzhou 221111, China*

Received: 09 November 2016 / Revised: 07 January 2017 / Accepted: 14 March 2017

Abstract: Medium manganese austenitic steel (MMAS) fabricated through the hot rolling process has been used in the mining, military, and mechanical industries. In this paper, the abrasion performance and hardening mechanism were measured under a series of impact energies. The impact wear was tested at different impact energies from 0.5 J to 6 J using a dynamic load abrasive wear tester (MLD-10). Microstructure and surface morphologies were analyzed using scanning electron microscopy, X-Ray diffraction, and transmission electron microscopy. The results suggest that MMSA has the best wear resistance at 3.5 J and the worst wear resistance at 1.5 J. Furthermore, the wear mechanism and worn surface microstructure change with different impact energies. There are small differences between a large amount of martensite on the worn surfaces under different impact energies and the shapes of dislocation and twins change with different impact energies.

Keywords: medium manganese steel; impact abrasion wear; work hardening; twin; martensite; dislocation

1 Introduction

Since Sir Robert Hadfield invented Hadfield's steel in 1882, high manganese austenitic steel has been used in the mining, military, and mechanical industries as a wear-resistant steel, given its excellent work hardening properties under high impact energy conditions [1]. Previous studies mainly focused on the high manganese austenitic steel with 1–1.4 wt% C and 10–14 wt% Mn, which has a good combination of high strength and ductility [2–4].

In 1963, to improve the work hardening properties under low impact energy conditions, the American Metal Climax company introduced a modified medium manganese wear-resistant steel [5]. Compared with Hadfield steel, medium manganese steel has a higher work-hardening capacity and a better wear-resistant performance under low-stress abrasive conditions [6]. The work hardening ability and the wear-resistant performance of austenitic medium manganese steel increase by 60%–120% (the highest surface hardness is up to 700 HV) and 50%–140%, respectively [7].

The work hardening mechanism and performance of medium manganese austenitic steel have been studied. Jing and Jiang [8] discovered that the high-rate work hardening of medium manganese steel under impact abrasion wear is due to the transformation of strain-induced martensite, but they did not research the effect of different impact energies on the work hardening mechanism and degree. Another work by Nakada et al. [9] investigated the differences between ferrite and austenite formations of medium manganese steel in transformation behaviors, which revealed the transformation behavior between γ to α and α to γ at the transition temperature, but did not reveal any work hardening mechanism apart from martensite transformation. To increase the surface hardness of medium manganese austenitic steel (MMAS), Xu [10]

* Corresponding author: Qingliang Wang, E-mail: wql889@cumt.edu.cn

investigated the process of eutectic growth in as-cast medium manganese steel and explained the mechanism of modularization of the eutectic. Wang et al. [11] studied nano-crystallization and α-martensite formation in the surface layer of medium manganese austenitic wear-resistant steel caused by shot peening, revealing that different depths from the shot-peened surface have different grain sizes and α-martensite. Xu et al. [12] studied heat treatment effects on the microstructure and mechanical properties of medium manganese steel.

In mining machinery, impact abrasion wear is one of the most prevalent causes of failure. Hence, it is important to evaluate the impact abrasion wear performance of wear-resistant materials. Although the impact abrasion wear test is a complicated model for analysis, it provides excellent guidance for actual production. The difference between the work hardening mechanism and the abrasion performance of medium manganese austenitic steel (MMAS) under different impact energies in impact abrasion wear has not been researched. In this study, we evaluated the abrasion performance and work hardening mechanism of MMAS (0.9 C–9 Mn) at different impact energies; the microstructure and topography of the worn surface were also analyzed. The mechanism of abrasion performance and work hardening mechanism at different impact energies has been discussed.

2 Materials and methods

2.1 Materials

Medium manganese austenitic steel (MMAS) was treated by hot rolling and water-toughening. Table 1 shows the chemical compositions of the steel. The microstructure of MMAS is full of austenite; the hardness and impact toughness (ak) are 260.3 HV and 137 J/cm^2, respectively.

2.2 Experimental procedure

The abrasion wear was tested using an abrasive wear test machine (MLD-10) with dynamic load, which is shown in Fig. 1. The samples for the abrasive wear test measured 10 mm × 10 mm × 30 mm and were mounted on a holder that was connected to the bottom of a hammer. The hammer drove the case sample falling onto the bottom sample. Driven by the continuously rotating eccentric wheel, the hammer was in reciprocating movement. A high-carbon chromium bearing steel (hardness: 350.3 HV) was used as the low counterpart sample with 200 rpm. When the hammer dropped, the samples were impacted on the bottom samples; abrasive particles were present between the case and counterpart sample during the entire process. The impact energies of wear tests were changed from 0.5 J to 6 J. It is calculated by the equation:

$$AK = G \cdot H$$

in which AK is the impact energy, G is the gravity of hammer, and H is the falling height of hammer. Samples were subjected to impact 6,000 times; the abrasion material was quartz sand between 8 and 12 mesh and a flux of 50 kg/h. For each condition, three test groups were tested and the wear of the samples was quantified by mass loss measurements.

The hardness of the worn surface was measured by a HV hardness tester (tested load: 1.96 N); each sample was tested five times. The topography of the worn surface was characterized by scanning electron microscopy (SEM, Hitachi S-3000) and the microstructure of the worn sample surface was characterized by transmission electron microscopy (TEM, Tecnai G2-T20) and X-ray diffraction (XRD, Rigaku-Ultima-III).

Table 1 Chemical composition of MMAS steel (wt%).

C	Mn	Si	Cr	V	Mo	S	P
0.9	9	0.6	2	0.15	0.3	< 0.02	< 0.02

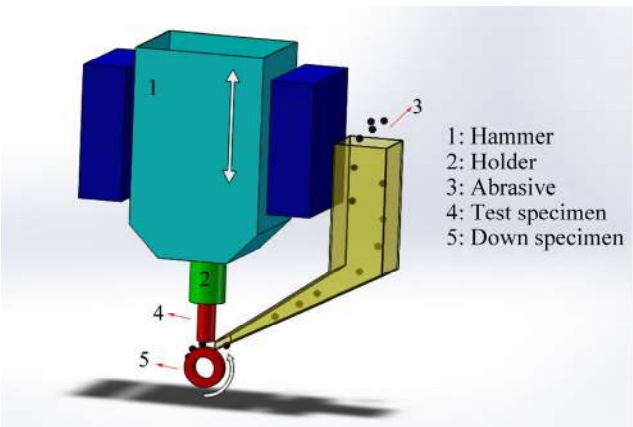

Fig. 1 Structure of the MLD-10.

3 Results

3.1 Abrasive wear performance

Figure 2 shows the relationship between the mass loss of the steel and impact energy for 6,000 impacts. As impact energy increases, the mass loss increases in the first (from 0.5 J to 1.5 J) and the third (from 3.5 J to 6.0 J) stages, while it decreases in the second stage (from 1.5 J to 3.5 J). MMAS shows the best abrasive wear resistance at the impact energy of 3.5 J and the worst wear resistance at the impact energy of 1.5 J. The mass loss of the 1.5 J impact energy sample is 259.02 mg, which is 1.78 times that at 3.5 J. The mass loss changes as the impact energy varies. The different wear performances of MMAS are attributed to the synthetic actions of surface hardness, work hardening degree, and wear mechanism influenced by the impact energy.

At lower impact energies (0.5–1.5 J), the impact stress of the wear layer is small and work hardening is not obvious. The mass loss caused by wear is greater than the effect of work hardening, which causes the mass loss to improve with the increase in impact energy. With increasing impact energy, the impact stress and work hardening of the wear layer increase significantly. The shear resistance of the wear layer improves, which reduces the cutting damage of abrasive particles to the wear layer. Consequently, the mass loss of wear reduces. When the impact energy exceeds 3.5 J, plastic deformation occurs in the wear layer under continued high cyclic stress. Crack initiation and propagation in the wear subsurface lead to fatigue fracture. Therefore, the mass loss of wear improves when the impact energy exceeds 3.5 J.

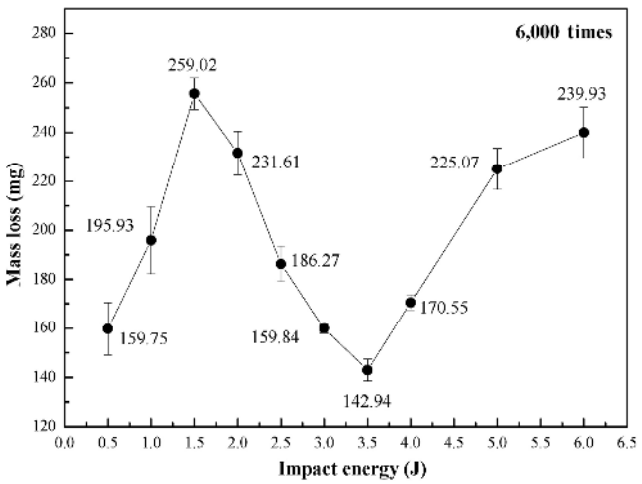

Fig. 2 The mass loss of the MMAS under different impact energies for 6,000 times.

3.2 Topography of the worn surface

Figure 3 shows the worn surface topographies of specimens at different impact energies. All surfaces are rough due to plastic deformation and the repeated impact of quartz sand. However, failure features of surface topography vary with the increase of the impact energy; there are mainly cuts, gouging pits, and plowing at 1 J, 1.5 J, and 2.5 J (Figs. 3(a), 3(b), and 3(c)), but it changes to fatigue spall at 3.5 J and 5 J (Figs. 3(d) and 3(e)). In addition, the cut pit at 1.5 J is larger and deeper than that at 1 J, and the fatigue spall of sample at 5 J is larger than that at 3.5 J.

3.3 Hardness of the worn surface

The hardness of the worn surface at different impact energies is shown in Fig. 4. As the impact energy increases, the hardness of the worn surface increases and it fluctuates around 575 HV when the impact energy exceeds 3.5 J. The hardness of the matrix is 260.3 HV, but the surface hardness increased to 385.3 HV at 0.5 J and the hardest surface is 587.6 HV when the impact energy is 3.5 J.

3.4 Subsurface hardness

Figure 5 shows the subsurface hardness of the sample at different impact energies (1 J–5 J). The work hardening degree is different at different impact energies. The work hardening depth is largest (about 2,200 μm) when the impact energy is 2.5 J; when impact energy exceeds 2.5 J, the depth is invariable. The subsurface hardness 50 μm from the surface at 2.5 J is 418.5 HV, and they are 421.2 HV, 440.3 HV, 464.6 HV, and 455.7 HV at 1 J, 1.5 J, 3.5 J, and 5 J, respectively. Though the hardness 50 μm from the surface at 2.5 J is smaller than those at 3.5 J and 5 J, the work hardening depth is approximate at 3.5 J and 5 J. In contrast, the work hardening depths of 1 J and 1.5 J are only 400 μm, in contrast with the samples whose impact energies exceeded 2.5 J.

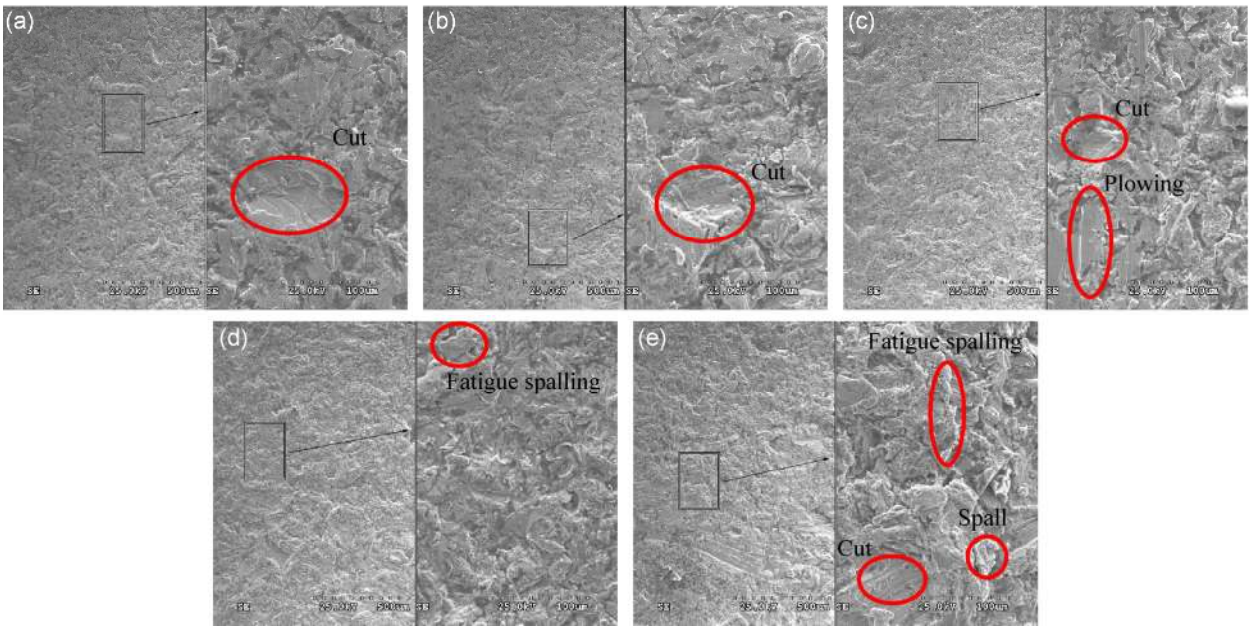

Fig. 3 The topography of the worn surface: (a), (b), (c), (d), and (e) are at 1 J, 1.5 J, 2.5 J, 3.5 J, and 5 J, respectively.

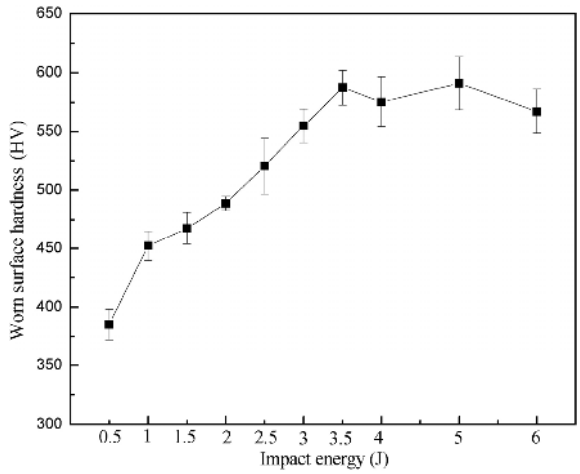

Fig. 4 The hardness of the worn surface.

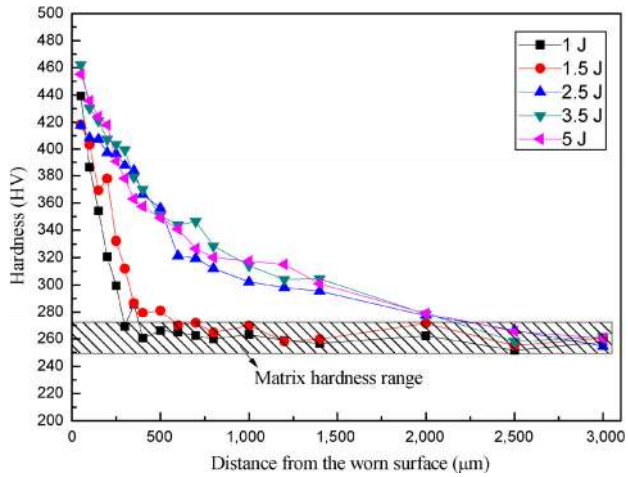

Fig. 5 The hardness of the subsurface.

3.5 The XRD results of the worn surface

The XRD patterns of the worn surface are shown in Fig. 6. The patterns for different impact energies are approximate, and there are two low intensity diffraction peaks indexed as bcc α-martensite besides three dominant peaks of fcc austenite.

Table 2 shows the amount of martensite on the worn surface. As shown, the amount of martensite accumulates slowly with the increase in impact energy. Compared with the maximum (35.9) and minimum (31.3) amounts of martensite at 4 J and 0.5 J, it can be seen that martensite transformation is approximate at

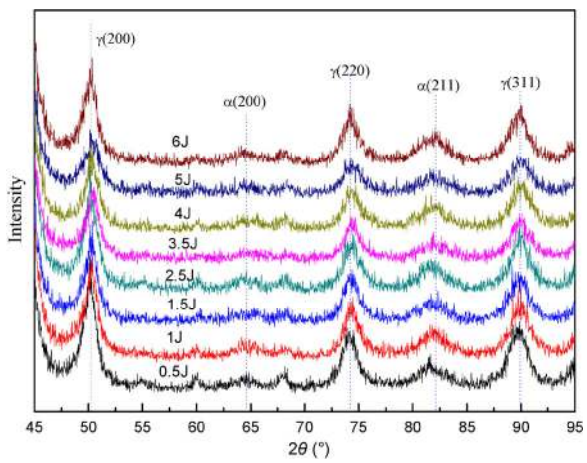

Fig. 6 XRD results of the worn surface under different impact energies from 0.5−6 J.

Table 2 The amount of martensite on worn surfaces.

Condition	0.5 J	1 J	1.5 J	2.5 J	3.5 J	4 J	5 J	6 J
Amount of martensite%	31.3	32.1	33.8	33.2	35.5	35.9	34.7	35.2

different impact energies and the martensite amount is stable when the impact energy exceeds 3.5 J.

3.6 TEM results of the worn surface

The microstructure of the subsurface is shown in Fig. 7. Figures 7(a) and 7(b) illustrate the TEM results at 1.5 J, while Figs. 7(c) and 7(d) are those at 3.5 J. Figure 7(a) shows a lath α-martensite in the austenite grain, and in Fig. 7(b) parallel acicular twins with stacking fault and dislocation wall are presented. In Fig. 7(c), there are lath twins accumulated together broader than those at 1.5 J. The α-martensite and island of dislocation are shown in Fig. 7(d), the shape of the dislocation is different from that at 1.5 J and the density of the dislocation in Fig. 7(d) is larger than that in Fig. 7(b).

4 Discussion

4.1 The wear performance and mechanism

The wear mechanism can be divided into three types: plowing, cutting, and wedge formation [13, 14]. In all abrasive wear modes, only the cut mode causes the removal of material; plowing and wedge formation lead to plastic deformation of the materials, which causes fatigue crack propagation. Hence, the wear performance strongly depends on the wear modes that are influenced by the mechanical property and abrasion conditions. In this study, the wear mechanism and hardness of the worn surface vary when the impact energy increases. When the impact energy is smaller than 2.5 J, the wear mode is mainly cutting; when the impact energy exceeds 2.5 J, it is mainly wedge formation. The multiply plastic deformation causes fatigue spall on the worn surfaces. Different wear mechanisms are caused by variation of the work hardening degree and the impact energy.

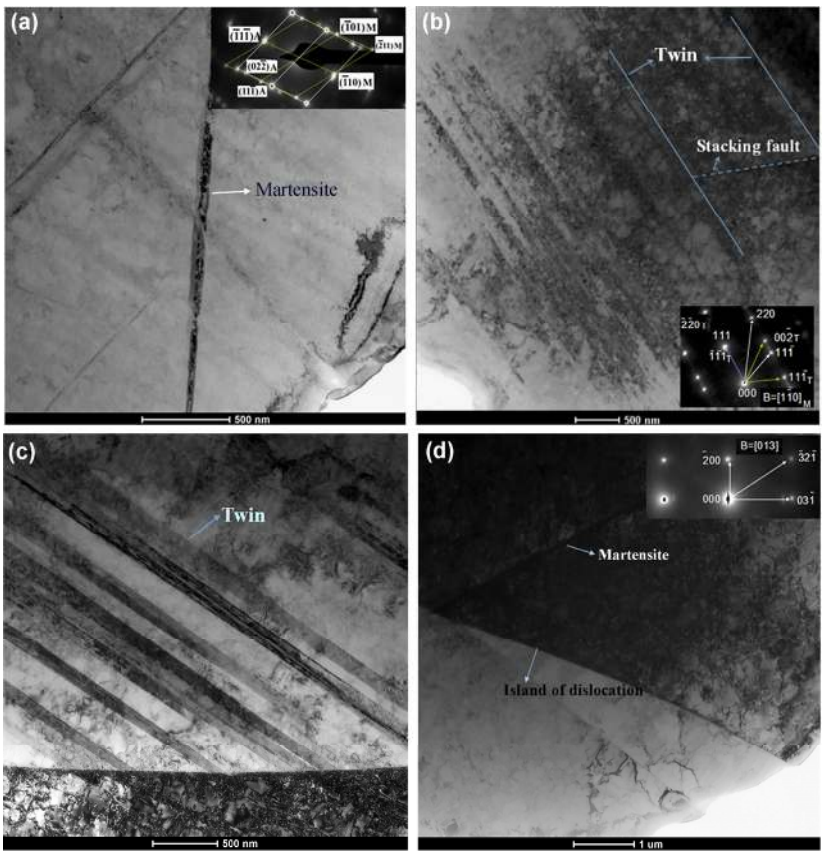

Fig. 7 The TEM results of the worn surface: (a) and (b) are the sample tested at 1.5 J impact energy; (c) and (d) are the sample tested at 3.5 J impact energy.

The difference between the worn surface's work hardening degree and work hardening depth are attributed to differences in the impact energies of the samples. Ojala et al. found that the work hardening and mechanical performance have a significant effect on wear performance [14].

As the impact energy increases from 0.5 J to 1.5 J, the worn surface hardness and work hardening depth accumulate slowly. The worn surface of the sample shows plowing and cutting when the impact energy is less than 1.5 J. In addition, the cut area and depth at 1.5 J are larger than those at 1 J due to the increase in impact energy. Therefore, the mass loss of MMAS increases with increasing impact energy in the first stage (from 0.5 J to 1.5 J).

In the second stage (from 1.5 J to 3.5 J), the work hardening degree increases with increasing impact energy. Although the hardness depths at 2.5 J and 3.5 J are similar, the surface hardness at 2.5 J is smaller than that at 3.5 J. With the increasing hardness of the surface and subsurface, the cut of the worn surface reduces so the mass loss decreases with increasing impact energy in the second stage.

The work hardening degree and hardening depth get saturated when the impact energy exceeds 3.5 J, but the strain increases with increasing impact energy. The multiply plastic deformation causes fatigue spall, so the surface is worn much easier with increasing impact energy. The pit and wedge formation increase and the mass loss increases when the impact energy exceeds 3.5 J, which leads to the increasing mass loss in the third stage (from 3.5 J to 6 J).

4.2 The work hardening mechanism

Allain et al. [15] and Dumay et al. [16] discovered that the plasticity mechanism changes with the variation of the stacking fault energy (SFE) as follows. It shows phase transformation when the SFE is less than 12 mJ/m^2 and the combined action of phase transformation and twinning when the SFE is between 12 mJ/m^2 and 18 mJ/m^2. There is twinning when the SFE is between 18 mJ/m^2 and 35 mJ/m^2, and slipping of the dislocation when the SFE exceeds 35 J/m^2. The SFE of MMAS has been calculated to be 16 mJ/m^2 [16–18], so the plastic deformation mechanism of austenitic steel is mainly twinning and phase transformation. Generally, materials with low SFE favor the twinning mechanism since the critical shear stress for twinning decreases with decreasing SFE, especially at high strain rates or low temperatures [19]. As shown above, variations of the worn surface's hardness and microstructure are presented at different impact energies. From the TEM results, the martensite transformation and the twinning are both indicated in the austenite grain at different impact energies.

At 1.5 J and 3.5 J, the amounts of martensite are 33.8% and 35.5%, respectively, and the hardness is 467.4 HV and 578.6 HV, respectively. It is observed that as the impact energy increases, the hardness accumulates and the amount of martensite measured is approximate. Therefore, martensite transformation is not the single key to the work hardening mechanism of MMAS.

Figure 8 shows the schematic summary of the microstructure features at different impact energies. With the increase of impact energy, the density of dislocations increases steeply, changing from cell to island and the twins are wider. The twin structure cuts the matrix and increases the strength [20]. The high density dislocation entanglement blocks the sliding of dislocations, which increases the plastic deformation resistance. So different shapes of dislocation and twins result at different degrees of work hardening. The different shapes of twins at different impact energies are caused by the different twin forming mechanisms.

The twin forming mechanism varies at different impact energies under two conditions. In Fig. 7(b), the twins are thin and there are stacking faults; the forming mechanism is self-partial-multiplication, which develops the twins by the reaction of the Shockley dislocation. In this forming mechanism, the Shockley should be located within the stacking fault, which is

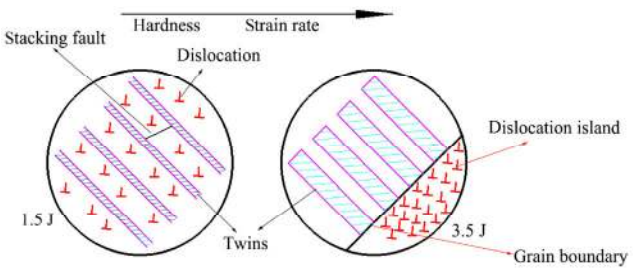

Fig. 8 Schematic summarizing the feature of twins and dislocation at different impact energies.

shown in Fig. 7(b). The twins at 3.5 J impact energy (Fig. 7(c)) are different from those at 1.5 J connected to the grain boundary, and the twin forming mechanism is the rebound mechanism in which the twin is produced by the rebounding of partial dislocations on the grain boundary. The two different twin forming mechanisms occur at different conditions: the rebound mechanism requires high strain rate and high stress but the self-partial-multiplication mechanism occurs at lower strain rate and stress [21]. The strain rates and stress increase with increasing impact energy. Therefore, the mechanism of twin forming shows variations at different impact energies. At high impact energy (3.5 J), the number of nucleation points and nucleation kinetics are higher than that at low impact energy (1.5 J), so the twins at 3.5 J are wider and denser. At the same time, the dislocation reproduces faster at higher impact energy than at lower impact energy due to the higher strain rate and stress. In addition, the dislocations entangle in the sliding process of plastic deformation. Therefore, the density of dislocations at 3.5 J is higher than at 1.5 J.

The different impact energies cause the variation in work hardening mechanisms, which determines the work hardening degree. In addition, work hardening degree and impact energy influence the wear mechanism of the worn surface. Finally, under the influence of wear mechanism and impact energy, the wear performance of MMAS varies at different impact energies.

5 Conclusions

In this paper, by using impact abrasion test methods at different impact energies, the abrasion resistance of the MMAS was evaluated by XRD, TEM, SEM, etc.

(1) In impact abrasion wear tests, the impact energy has a significant effect on the abrasion resistance of the steel. MMAS shows the best abrasion resistance at 3.5 J and worst abrasion resistance at 1.5 J.

(2) The wear modes of MMSA in impact abrasion wear tests are the combination of plowing, cutting, and fatigue spall. The wear modes vary at different impact energies. Cuts are the main wear mode at low impact energies, while fatigue spall is the main wear mode at high impact energies.

(3) MMSA has better hardening performance at 3.5 J; however, α-martensite transformation has the maximum limitation with increasing impact energy. Therefore, the shapes of twins and dislocations are the important work hardening mechanisms.

Acknowledgements

The present authors appreciate the financial support from the National Key Technology Support Program of China (Grant No. 2013BAEL3B00), Jiangsu Key Laboratory of Large Engineering Equipment Detection and Control (Grant No. JSKLEDC201403), the Fundamental Research Funds for the Central Universities (2015XKZD01), and National Basic Research Program of China (Project No. 2014CB046303).

Reference

[1] Michalon D, Mazet G, Burgio C. Manganese steel for abrasive environments: A conditioning process for Hadfield's manganese steel and a novel method of producing FAM bearings from the same material. *Tribol Int* **9**: 171–178 (1976)

[2] Efstathiou C, Sehitoglu H. Strain hardening and heterogeneous deformation during twinning in Hadfield steel. *Acta Mater* **58**: 1479–1488 (2010)

[3] Karaman I, Sehitoglu H, Gall K, Chumlyakov Y I, Maier H J. Deformation of single crystal Hadfield steel by twinning and slip. *Acta Mater* **48**: 1345–1359 (2000)

[4] Canadinc D, Sehitoglu H, Maier H J, Chumlyakov Y I. Strain hardening behavior of aluminum alloyed Hadfield steel single crystals. *Acta Mater* **53**: 1831–1842 (2005)

[5] Di X, Deng S, Wang B. Effect of pulse current on mechanical properties and dendritic morphology of modified medium manganese steel welds metal. *Mater Design* **66**: 169–175 (2015)

[6] Jost N, Schmidt I. Friction-induced martensitic transformation in austenitic manganese steels. *Wear* **111**: 377–389 (1986)

[7] He Z, Jiang Q, Fu S, Xie J. Improved work-hardening ability and wear resistance of austenitic manganese steel under non-severe impact-loading conditions. *Wear* **120**: 305–319 (1987)

[8] Jing T, Jiang F. The work-hardening behavior of medium manganese steel under impact abrasive wear condition, *Mater Lett* **31**: 275–279 (1997)

[9] Nakada N, Mizutani K, Tsuchiyama T, Takaki S. Difference in transformation behavior between ferrite and austenite formations in medium manganese steel. *Acta Mate* **65**: 251–258 (2014)

[10] Xu Z. Eutectic growth in as-cast medium manganese steel. *Mat Sci Eng A-Struct* **335**: 109–115 (2002)

[11] Wang T S, Lu B, Zhang M, Hou R J, Zhang F C. Nanocrystallization and α-martensite formation in the surface layer of medium-manganese austenitic wear-resistant steel caused by shot peening. *Mat Sci Eng A-Struct* **458**: 249–252 (2007)

[12] Xu H F, Zhao J, Cao W Q, Shi J, Wang C Y, Wang C, Li J, Dong H. Heat treatment effects on the microstructure and mechanical properties of a medium manganese steel (0.2C–5Mn). *Mat Sci Eng A-Struct* **532**: 435–442 (2012)

[13] Hokkirigawa K, Kato K. An experimental and theoretical investigation of ploughing, cutting and wedge formation during abrasive wear. *Tribol Int* **21**: 51–57 (1988)

[14] Khun N W, Liu E, Tan A W Y, Senthilkumar D, Albert B, Lal D M. Effects of deep cryogenic treatment on mechanical and tribological properties of AISI D3 tool steel. *Friction* **3**: 234–242 (2015)

[15] Ojala N, Valtonen K, Heino V, Kallio M, Aaltonen J, Siitonen P, Kuokkala V T. Effects of composition and microstructure on the abrasive wear performance of quenched wear resistant steels. *Wear* **317**: 225–232 (2014)

[16] Allain S, Chateau J P, Bouaziz O, Migot S, Guelton N. Correlation between the calculated stacking fault energy and the plasticity mechanism in Fe–Mn–C alloys. *Mat Sci Eng A-Struct* **378–389**: 158–162 (2004)

[17] Dumay A, Chateau J P, Allain S, Migot S, Bouaziz O. Influence of addition elements on the stacking-fault energy and mechanical properties of a austenitic Fe-Mn-C steel. *Mat Sci Eng A-Struct* **483–484**: 184–187 (2008)

[18] Li L, Hsu T Y. Gibbs free energy evaluation of the fcc(γ) and hcp(ε) phases in Fe-Mn-Si alloys. *Calphad* **21**: 443–448 (1997)

[19] Zhang J, Liu G, Wei X. Strengthening and ductilization potentials of nonmetallic solutes in magnesium: First-principles calculation of generalized stacking fault energies. *Mater Lett* **150**: 111–113 (2015)

[20] Jin J E, Lee Y K. Strain hardening behavior of a Fe–18Mn–0.6C–1.5Al TWIP steel. *Mat Sci Eng A-Struct* **527**: 157–161 (2009)

[21] Zhu Y T, Narayan J, Hirth J P, Mahajan S, Wud X L, Liao X Z. Formation of single and multiple deformation twins in nanocrystalline fcc metals. *Acta Mate* **57**: 3763–3770 (2009)

Hui CHEN. He received his bachelor and M.S. degrees in material science and engineering in 2006 from China University of Mining and Technology, Xuzhou, China. After then, he was a Ph.D student in the Chemical Technology School at the same university. He has recently obtained his Ph.D. degree in mineral materials engineering at China University of Mining and Technology. His research interests include wear-resistance steel, fuel cell, and nano composite materials.

Qingliang WANG. He received M.S. degree in metallurgy and material engineering from Chongqing University, China, in 1992. After then, he received his Ph.D. degree in mechanical engineering from China University of Mining and Technology, China, in 2004. He joined Institute of Tribology and Reliability Engineering at China University of Mining and Technology from 1992. His current position is a professor and his research areas include biological materials, surface engineering, and tribology of composite materials.